Inverse Problems and Imaging
Volume 00, No. 0, 2009, 1–9

Web site: http://www.aimSciences.org

SYNTHETIC FOCUSING IN ULTRASOUND MODULATED TOMOGRAPHY

Peter Kuchment

Mathematics Department, Texas A&M University
College Station, TX 77843-3368, USA

Leonid Kunyansky

Mathematics Department, University of Arizona
Tucson, AZ 85721, USA

(Communicated by the associate editor name)

Abstract. Several hybrid tomographic methods utilizing ultrasound modulation have been introduced lately. Success of these methods hinges on the feasibility of focusing ultrasound waves at an arbitrary point of interest. Such focusing, however, is difficult to achieve in practice. We thus propose a way to avoid the use of focused waves through what we call *synthetic focusing*, i.e. by reconstructing the would-be response to the focused modulation from the measurements corresponding to realistic unfocused waves. Examples of reconstructions from simulated data are provided. This non-technical paper describes only the general concept, while technical details will appear elsewhere.

Introduction

The last decade has seen the proliferation of the so called hybrid methods of medical imaging, where different physical types of radiation are combined into one tomographic process (e.g., [6, 13, 15, 16, 21, 28, 29, 31, 33]). Such a combination allows one to alleviate deficiencies of each separate type of waves, while combining their strengths. Thermoacoustic (and closely related photoacoustic) tomography is an example of such a hybrid method (see [2, 11, 16, 27–29, 31, 33] and references therein).

In this text we discuss a very specific type of hybrid imaging, the one that combines electrical or optical measurements with a concurrent scanning of the object with ultrasound (US) waves. The propagating US wave slightly modifies the local physical properties of the medium, such as its electrical conductivity or the distribution of light scatterers. This, in turn, perturbs the background tomographic measurements (electric or optical). These perturbations are measured and used to reconstruct the electrical or optical properties of the medium. Such hybrid methods hold a promise to improve the tomographic modalities that are otherwise notorious for their instability and/or low resolution, such as electrical impedance tomography [9] or optical imaging [31]. For these hybrid methods we will use the names

2000 *Mathematics Subject Classification:* Primary: 44A12, 92C55; Secondary: 65R32.

Key words and phrases: Radon transform, spherical means, thermoacoustic tomography, optical tomography, impedance tomography.

Acousto-Electric Tomography (AET) and Ultrasound Modulated Optical Tomography (UMOT)[1].

It has been understood that if one could focus the ultrasound on a small spot inside the body, knowledge of this location would have a stabilizing effect on the reconstruction in otherwise highly unstable imaging modalities (see e.g. [5, 7] and Section 2.2.3 below). In this text, however, our goal is not to discuss the ultrasound modulated imaging in detail, but rather to address the assumption of a well focused US beam. It is known that such focusing (to the extent needed for tomography) is hard to achieve (see, for example, the detailed discussion of this issue in [14]). Thus, it would be important to find a way of utilizing instead unfocused US waves. As we will show, this can be achieved through synthetic focusing, i.e. by extracting the measurements corresponding to well-focused beams, from the data obtained with unfocused waves. Under such approach, the tomographic problem is solved in two steps (hopefully both stable): first, synthetic focusing, and then inversion from the "focused" beam data. We will not attempt to address the second step in this short text (see [5, 7, 17] where the various implementations of such a procedure are discussed). Instead, we show that the first step (synthetic focusing), under appropriate choice of waves, is stable and mathematically equivalent to the reconstruction in thermoacoustic tomography (although no thermoacoustic measurements are conducted). In some cases, this step can even be reduced to the inversion of the Fourier transform. An example of the AET reconstruction is also provided.

This paper is meant as a preliminary non-technical announcement, which follows a part of the lecture given at the Jan Boman's conference "Integral Geometry and Tomography" in August 2008. The technical analytic and numerical details will be provided elsewhere.

The structure of the paper is as follows: The idea of US modulation in tomography is summarized in Section 1. Section 2 contains the description of four different types of unfocused US waves that one might try to use. In each case it is shown that the synthetic focusing (within the assumed mathematical model approximation) reduces to one of the well known analytic reconstruction procedures. Section 2.2.3 is devoted to a brief description of the AET procedure and a numerical example. Remarks are contained in Section 3, followed by Acknowledgments and References.

1. Ultrasound modulation in tomography

As indicated in the Introduction, the ultrasound (US) modulation in various types of tomography is performed by sending a US wave through the object, concurrently with the original tomographic measurement (say, optical or electric). Varying the shape of the wave, one observes the resulting changes in the tomographic data and tries to extract from them the quantity of interest. This technique promises to improve significantly the stability of such modalities as electrical impedance tomography (EIT) and optical tomography (OT).

To be more specific, let us consider the EIT case [2], where one seeks to recover the conductivity $\sigma(x)$ inside of an object occupying the domain Ω from boundary impedance measurements. Assume for instance that a boundary current $g(y)$ is applied and one measures the corresponding boundary potential response $h(z)$. Here y and z denote variable points on the boundary $\partial\Omega$. In EIT, the current g is varied and the potential h is measured, so that the complete Neumann-to-Dirichlet operator

[1] Other names have also been used [6, 7, 31].

[2] The first AET reconstructions were probably suggested and implemented in [34].

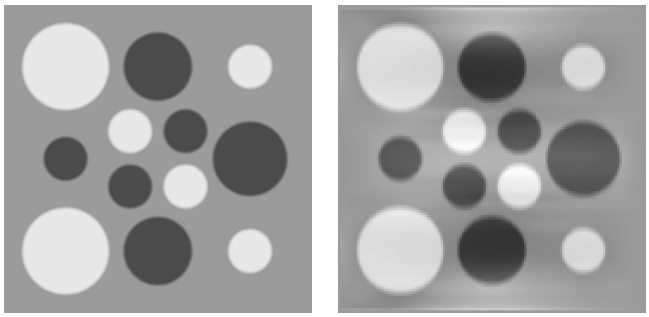

(a) Phantom (b) Reconstruction

Figure 1. Phantom and its EIT reconstruction using focused US modulation.

Λ_σ on $\partial\Omega$ is obtained (alternatively, by varying h, one recovers the Dirichlet-to-Neumann operator). In the case of ultrasound modulation (at least in the example discussed in Section 2.2.3), a single boundary current can be used, rather than the whole operator Λ_σ; we will thus assume that g is fixed. Suppose now that, given any point $x \in \Omega$, we could create a US wave that would approximate well the delta function at the location x. This would create a perturbation $h_x(y)$ of the original boundary voltage $h(y)$. By scanning the focusing point x through the domain Ω, one obtains the set of functions $h_x, x \in \Omega$, from which one can try to recover the internal conductivity σ. This can actually be done, and the reconstruction does not inherit the original high instability of EIT (see the details in [7, 17], where two different approaches are presented). A somewhat similar situation arises in OT [5, 23, 24]. Stability of such reconstructions can be seen in Figures 1 and 2 (taken from [17] and [5] correspondingly). These figures show mathematical phantoms (left) and their reconstructions obtained using the simulated perfectly focused US modulations in EIT and OT correspondingly (images on the right).

No additional noise was introduced in the simulated data used in these examples besides the small error resulting from numerical approximation of the underlying PDE's. It is well known that even in the presence of such small errors, sharp features like material interfaces cannot be recovered well in traditional EIT and OT, unless some additional *a priori* information about the image (such as, for example, the image being piece-wise constant) is used. As clearly shown by the above examples, US modulation results in accurate reconstructions of the interfaces, which, in turn, implies stability of the hybrid modalities (the issues of stability will be discussed in more detail, along with the reconstruction methods, in [5, 17]).

However, as we have mentioned in the Introduction, the problem with this technique is the difficulty of physically generating well localized US waves (see e.g. [14]). We thus suggest the use of a synthetic focusing approach described in the next section.

2. Synthetic focusing

We start by mentioning that the acousto-electric and opto-acoustic effects that are responsible for the perturbations in the electric and optical properties of the medium due to US irradiation, are very small (e.g., [19, 20, 31, 34]). Although this makes the resulting boundary effects harder to measure, it also enables one to use

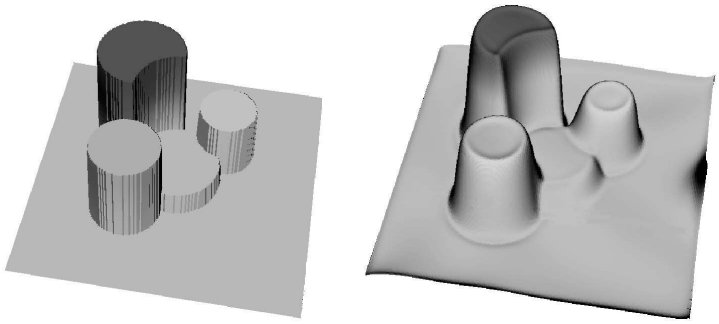

(a) Phantom (b) Reconstruction

FIGURE 2. Phantom and its OT reconstruction using focused US modulation.

the linearization of the problem in the following sense. Let $\sigma(x)$ be the parameter to be reconstructed, say, electrical conductivity in the EIT case. The perturbation $\delta\sigma$ of σ due to the applied US wave will be very small. Hence, one can safely assume that the operator L that maps the perturbation $\delta\sigma$ into the perturbation δh of the measured data h is linear. In fact, the operator L depends on the underlying σ and thus will be denoted as L_σ.

Due to smallness of the amplitude of the applied US wave, as well as the smallness of the acousto-electric and opto-acoustic effects, one can try also to linearize the effect of local pressure on the perturbation $\delta\sigma$. It turns out that such a linearization is possible in AET; it happens to be incorrect in the optical case, where the dependence is quadratic [31].

Let now

$$L_\sigma : \delta\sigma(x) \mapsto \delta h(y), x \in \Omega, y \in \Gamma \subset \partial\Omega \tag{1}$$

be the linear operator that maps the distributed perturbation $\delta\sigma(x)$ of the material parameter (say, conductivity) inside Ω to the perturbation $\delta h(y)$ of the tomographic data measured on a part Γ of the boundary $\partial\Omega$ (which, in principle, could consist of a single point, although this would not be advisable in tomography). If one could create US waves well localized at arbitrary locations $x \in \Omega$, this would allow one to measure the response of L to delta-type inputs, and thus would lead to a direct measurement of the kernel $l(x, y)$ of the operator L:

$$(Lf)(y) = \int_\Omega l(x, y)f(x)dx, x \in \Omega, y \in \Gamma. \tag{2}$$

So, the use of perfectly focused US waves is equivalent to measuring the kernel $l(x, y)$. The general idea of synthetic focusing is to use a more realistic non-localized complete set $w_\alpha(x)$ of US waves and to recover the kernel $l(x, y)$ from the measured responses

$$\int_\Omega l(x, y)w_\alpha(x)dx.$$

In other words, one reconstructs numerically the would-be response of the tomographic measurement to the perfectly focused US irradiation, which explains our use of the name "synthetic focusing".

We now address some specific versions of synthetic focusing in sub-sections below. (The reader should be warned that we discuss here only the reconstruction of the kernel $l(x,y)$, but not the procedure of the further recovery of $\sigma(x)$ from the kernel.)

2.1. SPHERICAL WAVES. Suppose that one places a point US transducer at arbitrary location $z \in \partial\Omega$ and creates a short impulse that approximates a spreading spherical wave $p(t,z,x) = \delta(|x-z| - vt)$, where v is the constant US speed in the tissue[3]. Then the response of the measurement operator L_σ produces the spherical integrals of the kernel $l(x,y)$

$$L_\sigma(p(t,z,\cdot)) = \int\limits_{|x-z|=vt} l(x,y)dx, z \in \partial\Omega. \tag{3}$$

We thus arrive to the problem of recovering a function $l(x,y)$ of x (y is now just a fixed parameter) inside domain Ω from known integrals from l over all spheres centered at the boundary $\partial\Omega$. This problem has been studied extensively, in particular due to its relevance for the thermoacoustic tomography (TAT); numerous results concerning the solvability, stability, and inversion methods have been obtained (see [1–4, 10–12, 16, 18, 27, 30, 31, 33]). In particular, when $\partial\Omega$ is a sphere, a variety of backprojection type formulas have been derived. We provide below the $3D$ formula derived in [32] (it was generalized to all dimensions in [18]):

$$f(x) = \frac{1}{8\pi^2}\mathrm{div}\int\limits_{\partial\Omega}\mathbf{n}(z)\left(\frac{1}{t}\frac{d}{dt}\frac{g(z,t)}{t}\right)\Bigg|_{t=|y-x|} dA(z). \tag{4}$$

Here Ω is the unit sphere, $g(y,t)$ is the average of l over the sphere centered at $y \in \partial\Omega$ and of radius t, $\mathbf{n}(y)$ is the outward normal vector to $\partial\Omega$ at y, and dA is the surface area measure.

Several different inversion formulas were derived earlier in [10] (see also an unified approach to such formulas in [25]).

In the case of non-spherical surfaces, eigenfunction expansions and time reversal methods can be used to reconstruct l (see [1, 2, 4, 10–12] and references therein).

2.2. SPHERICAL MONOCHROMATIC WAVES AND PLANE WAVES IN AET. Since in AET the electric response of the medium is proportional to the perturbation in the pressure, one can use for scanning not only acoustic pulses, but also monochromatic waves. Using such waves has the advantage that the resulting boundary measurement will oscillate with ultrasound frequency. Hence, its time Fourier transform allows one to selectively pick up this frequency, thus reducing the effects of the wide spectrum noise.

2.2.1. *Spherical monochromatic waves.* Suppose that the monochromatic wave $p_\lambda(t,z,x)$ with a time frequency λ is produced by a point transducer located at the point $z \in \partial\Omega$:

$$p_\lambda(t,z,x) = e^{-i\lambda t}\frac{e^{i\lambda|x-z|}}{4\pi|x-z|}.$$

[3]This certainly requires broadband transducers, as is the case in all other suggested synthetic focusing methods. Ultrawide-band transducers are commercially available with essentially uniform response in the range from 10KHz up to 20MHz, or even 100MHz [26, 33].

Then

$$(Lp_\lambda(t,z,\cdot))(y) = \int\limits_\Omega l(x,y)e^{-i\lambda t}\frac{e^{i\lambda|x-z|}}{4\pi|x-z|}dx, x\in\Omega, y\in\Gamma, z\in\partial\Omega,$$

and the Fourier transform with respect to time $\widehat{Lp_\lambda}(z,y)$ of Lp_λ will be equal to the integral of $l(x,y)$ multiplied by the free-space Green's function $\Phi_\lambda(x,z)$ of the Helmholtz equation:

$$\widehat{Lp_\lambda}(z,y) = \int\limits_\Omega l(x,y)\Phi_\lambda(x,z)dx,$$
$$\Phi_\lambda(x,z) = \frac{e^{i\lambda|x-z|}}{4\pi|x-z|}.$$

As before, we assume that the point y at which the electrical measurements are conducted, is fixed. Then, if the measurements are repeated for a wide range of frequencies λ and for all $z\in\partial\Omega$, and are followed by the inverse Fourier transform (in λ) applied to $\widehat{Lp_\lambda}(z,y)$, one recovers the integral of l over the spheres centered at z as in (3). Now the problem of recovering $l(x,y)$ from values of $\widehat{Lp_\lambda}(z,y)$ is equivalent to inverting the spherical mean Radon transform of l; such an inversion was discussed in the previous section.

Alternatively, since the first step of the reconstruction formulas presented in [18] consists in computing the values of $\widehat{Lp_\lambda}(z,y)$, one can reconstruct $l(x,y)$ without explicitly reconstructing the values of its spherical mean Radon transform first. In particular, by using the 3-D formula from [18], one obtains the following reconstruction formula for $l(x,y)$ from $\widehat{Lp_\lambda}(z,y)$:

$$l(x,y) = -\frac{1}{2\pi^2}\mathrm{div}_x \int\limits_{|z|=R} \mathbf{n}(z)h_y(z,|x-z|)dA(z),$$

with

$$h_y(\mathbf{z},t) = -\frac{1}{t}\int\limits_{\mathbb{R}^+}\left[\cos(\lambda t)\,\mathrm{Im}\left(\widehat{Lp_\lambda}(z,y)\right) - \sin(\lambda t)\,\mathrm{Re}\left(\widehat{Lp_\lambda}(z,y)\right)\right]\lambda d\lambda.$$

Here, as before, $\mathbf{n}(y)$ is the outward normal vector to $\partial\Omega$ at y, and dA is the surface area measure.

2.2.2. *Plane waves.* Spherical waves arise when the size of the transducer is small compared to the wavelength. If the distance from the transducer to the object of interest is much larger than the size of the object, the wave is approximately planar. Plane waves can also be created by using a large planar transducer. In either case the transducer should be broadband to permit generation of plane waves in a wide range of frequencies.

Measurement done using planar acoustic waves $p_k(t,z,x) = e^{-i|k|t}\exp(ik\cdot x)$ correspond to measuring the Fourier transform of the kernel $l(x,y)$:

$$\widehat{Lp_k}(z,y) = \int\limits_\Omega \exp(ik\cdot x)l(x,y)dx.$$

Synthetic focusing now reduces to the inversion of the Fourier transform.

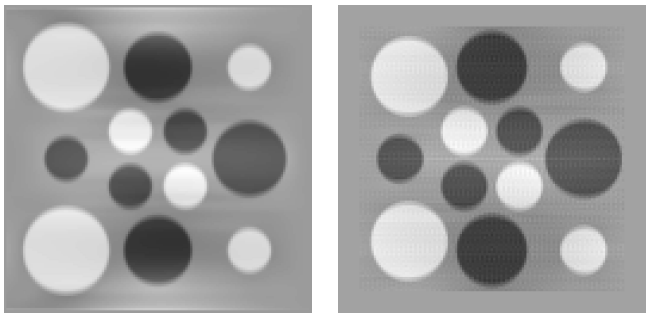

(a) Ideal focusing (b) Synthetic focusing

Figure 3. Comparison of AET reconstructions using ideal focusing (a) versus synthetic focusing (of spherical pulse waves) (b).

2.2.3. *Example of AET.* Let us illustrate by a numerical example the application of synthetic focusing to image reconstruction in AET. We simulated numerically a square domain, with the electrical currents equal 1 on the left and right sides of the square and 0 on the top and the bottom. The conductivity $\sigma(x)$ we used in our experiments was close to 1; the gray scale density plot of the logarithm $\log \sigma(x)$ is shown in Figure 1(a). In this figure the light circles correspond to the value $\log \sigma(x) = 0.05$, the dark ones represent the value of $\log \sigma(x) = -0.05$, and the gray background depicts $\log \sigma(x) = 0$. The simulated electric potential was "measured" on the whole boundary of the square.

As mentioned previously, Figure 1(b) presents the result of AET reconstruction from simulated measurements corresponding to perfectly focused US modulation. For convenience we repeat this image in Figure 3(a). The AET reconstruction of the same phantom, obtained by using synthetic measurements, is shown in Figure 3(b). In this example we modeled the perturbations of electric potential on the boundary caused by the spherical pulse waves with the centers on a circle surrounding our square domain. The total of 300 transducers and 800 different radii of outgoing spherical pulses per transducer were simulated. The reconstruction shown in Figure 3(b) was computed by using synthetic focusing to obtain $l(x, y)$ and then by reconstructing conductivity $\sigma(x)$ (again, the methods for reconstructing σ from l will be discussed elsewhere.) As before, no noise was added to simulated measurements. The reconstructed image is clearly as good as the one obtained using the perfectly focused US modulation (3(a)).

2.3. Elongated focusing areas and X-ray transform. One of the UMOT reconstruction methods, suggested in [22] (see also [31]), appears to be, in fact, synthetic focusing rather than a true reconstruction. The authors of [22] employed the observation that the focusing was non-perfect: the focal zone of the ultrasonic waves was 2 mm across and 20 mm in length, which made it a better approximation to a segment rather than a point. As far as we understood the procedure of [22], by shifting and rotating the focusing area, an approximation to the X-ray transform of the kernel $l(x, y)$ (as before, with respect to the variable x) was obtained. Then standard X-ray inversion formulas were used to recover the kernel l, which was treated as the image.

3. Remarks

1. As has already been mentioned, exact analytic and numerical details of the reconstruction procedures will be provided elsewhere.
2. Practical implementation of the suggested synthetic focusing procedures will have to include more precise information about possibilities and imperfections of the currently available transducers.
3. The UMOT situation differs from AET and will probably not allow usage of monochromatic US modulation. However, the modulation by spherical pulse waves should still be possible. These issues will be addressed elsewhere. (As has been already mentioned, synthetic focusing using X-ray transforms was implemented for UMOT in [22, 31].)

Acknowledgments

The work of the first author was partially supported by the NSF DMS grant 0604778 and by the KAUST grant KUS-CI-016-04. The work of the second author was partially supported by the DOE grant DE-FG02-03ER25577. The authors express their gratitude to NSF, DOE, and KAUST for the support. The authors also thank M. Allmaras, G. Bal, W. Bangerth, J. Schotland, L.-H. Wang, Y. Xu, and the referee for useful information and discussions. We are grateful to M. Allmaras and W. Bangerth for allowing us to use Fig. 2.

References

[1] M. Agranovsky and P. Kuchment, *Uniqueness of reconstruction and an inversion procedure for thermoacoustic and photoacoustic tomography with variable sound speed*, Inverse Problems **23** (2007), 2089–2102.

[2] M. Agranovsky, P. Kuchment, and L. Kunyansky, *On reconstruction formulas and algorithms for the thermoacoustic and photoacoustic tomography*, Ch. 8 in [30], 89–101.

[3] M. Agranovsky, P. Kuchment, and E. T. Quinto, *Range descriptions for the spherical mean Radon transform*, J. Funct. Anal. **248** (2007), 344–386.

[4] M. Agranovsky and E. T. Quinto, *Injectivity sets for the Radon transform over circles and complete systems of radial functions*, Journal of Functional Analysis **139** (1996), 383–414.

[5] M. Allmaras, W. Bangerth, and P. Kuchment, *On reconstructions in ultrasound modulated optical tomography*, in preparation.

[6] H. Ammari, "An Introduction to Mathematics of Emerging Biomedical Imaging", Springer-Verlag, 2008.

[7] H. Ammari, E. Bonnetier, Y. Capdeboscq, M. Tanter, and M. Fink, *Electrical impedance tomography by elastic deformation*, SIAM J. Appl. Math. **68** (2008), 1557–1573.

[8] D. C. Barber, B. H. Brown, *Applied potential tomography*, J. Phys. E.: Sci. Instrum. **17**(1984), 723–733.

[9] L. Borcea, *Electrical impedance tomography*, Inverse Problems **18** (2002), R99–R136.

[10] D. Finch, S. Patch, and Rakesh, *Determining a function from its mean values over a family of spheres*, SIAM J. Math. Anal. **35** (2004), no. 5, 1213–1240.

[11] D. Finch and Rakesh, *The spherical mean value operator with centers on a sphere*, Inverse Problems **23** (2007), S37–S50.

[12] D. Finch and Rakesh, *Recovering a function from its spherical mean values in two and three dimensions* To appear in [30].

[13] B. Gebauer and O. Scherzer, *Impedance-Acoustic Tomography*, preprint http://pai.uibk.ac.at, 2008.

[14] H. E. Hernandez-Figueroa, M. Zamboni-Rached, and E. Recami (Editors), "Localized Waves", IEEE Press, J. Wiley & Sons, Inc., Hoboken, NJ 2008.

[15] M. Kempe, M. Larionov, D. Zaslavsky, and A. Z. Genack. *Acousto-optic tomography with multiply scattered light*, J. Opt. Soc. Am. A **14** (1997), 1151–1158.

[16] P. Kuchment and L. *Kunyansky, Mathematics of thermoacoustic tomography*, European J. Appl. Math., **19** (2008), Issue 02, 191–224.
[17] P. Kuchment and L. Kunyansky, *Ultrasound modulated electric impedance tomography*, in preparation.
[18] L. A. Kunyansky, *Explicit inversion formulae for the spherical mean Radon transform*, Inverse Problems **23** (2007), pp. 373–383.
[19] B. Lavandier, J. Jossinet and D. Cathignol, *Quantitative assessment of ultrasound-induced resistance change in saline solution*, Medical & Biological Engineering & Computing **38** (2000), 150–155.
[20] B. Lavandier, J. Jossinet and D. Cathignol, *Experimental measurement of the acousto-electric interaction signal in saline solution*, Ultrasonics **38** (2000), 929–936.
[21] J. Li and L.-H. Wang, *Methods for parallel-detection-based ultrasound-modulated optical tomography*, Applied Optics **41** (2002), 2079–2084.
[22] J. Li and L.-H. *Wang, Ultrasound-modulated optical computed tomography of biological tissues*, Appl. Phys. Lett. **84** (2004), 1597–1599.
[23] H. Nam. "Ultrasound modulated optical tomography", Ph.D thesis, Texas A&M University, 2002.
[24] H. Nam and D. Dobson, *Ultrasound modulated optical tomography*, preprint 2004.
[25] Linh V. Nguyen, A family of inversion formulas in thermoacoustic tomography, preprint arXiv:0902.2579.
[26] A. A. Oraevsky and A. A. Karabutov, 2003 *Optoacoustic Tomography*, in [29], 34-1 – 34-34.
[27] S. K. Patch and O. Scherzer, *Photo- and thermo-acoustic imaging (Guest Editors' Introduction)*, Inverse Problems **23** (2007), S01–S10.
[28] V. V. Tuchin (Editor), "Handbook of Optical Biomedical Diagonstics", SPIE, Bellingham, WA 2002.
[29] T. Vo-Dinh (Editor), "Biomedical Photonics Handbook", edited by CRC, Boca Raton, FL 2003.
[30] L. H. Wang (Editor), "Photoacoustic imaging and spectroscopy", CRC Press 2009.
[31] L. V. Wang and H. Wu, "Biomedical Optics. Principles and Imaging", Wiley-Interscience 2007.
[32] M. Xu and L.-H. V. Wang, *Universal back-projection algorithm for photoacoustic computed tomography*, Phys. Rev. E **71** (2005), 016706.
[33] M. Xu and L.-H. V. Wang, *Photoacoustic imaging in biomedicine*, Review of Scientific Instruments **77** (2006), 041101-01 – 041101-22.
[34] H. Zhang and L. Wang, *Acousto-electric tomography*, Proc. SPIE 5320 (2004), 145–149.

Received January 2009; revised May 2009.

E-mail address: kuchment@math.tamu.edu
E-mail address: leonk@math.arizona.edu